Fuel 383 (2025) 133848

Contents lists available at ScienceDirect

Fuel

journal homepage: www.elsevier.com/locate/fuel

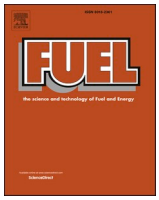

Full Length Article

Structure-Reactivity- and Modelling-Relationships during Thermal Annealing in Biomass Entrained-Flow Gasification: The Effect of Temperature and Residence Time

Weiss Naim [a,*], Philipp Treu [b], Matthias Dohrn [d], Erisa Saraçi [b,c], Jan-Dierk Grunwaldt [b,c], Sebastian Fendt [a], Hartmut Spliethoff [a]

[a] Technical University of Munich TUM, Chair of Energy Systems (CES), Boltzmannstrasse 15, 85748 Garching, Germany
[b] Karlsruhe Institute of Technology KIT, Institute of Catalysis Research and Technology (IKFT), Hermann-von-Helmholtz-Platz1, 76344 Eggenstein-Leopoldshafen, Germany
[c] Karlsruhe Institute of Technology KIT, Institute for Chemical Technology and Polymer Chemistry (ITCP), Engesserstrasse 20, 76131 Karlsruhe, Germany
[d] RWE Power AG, Research and Development, Werkstrasse, 50129 Bergheim, Germany

ARTICLE INFO

Keywords:
Gasification
Pyrolysis
Reactivity
Annealing
Char Characterization

ABSTRACT

Biomass entrained-flow gasification enables the sustainable production of chemicals and liquid fuels. For reliable and accurate gasifier operation and design, the analysis of biomass char reactivity represents one of the key studies. Therefore, the annealing-induced char reactivity loss needs to be investigated for biogenic feedstocks from microscopic to reactor level. In the present work, the influence of pyrolysis temperature and particle residence time on solid digestate char reactivity and structure is studied. Several char types are prepared in a pressurized entrained-flow reactor between 1200 °C and 1600 °C with varying residence times between 0.4–2.4 s. Isothermal char reactivity in O_2 and CO_2 atmosphere is measured by TGA and reactivities are determined. Strong char deactivation between 1200 °C and 1400 °C resulted from severe heat treatment, especially toward the CO_2 reaction. At 1600 °C, the influence of residence time becomes less relevant since all measured reactivities are comparably low. Experimental data are fitted to a coal deactivation model and verified for biogenic residues with very good agreement. The results are further corroborated by char structure analysis using FT-IR, XRD, Raman spectroscopy, SEM-EDX and ETV-ICP-OES. The decrease in char reactivity is mainly attributed to graphitization and the formation of aromatic ring structures. Char deactivation is further promoted by the loss of catalytic mineral matter and by high concentrations of inhibiting elements like phosphorus.

1. Introduction

The utilization of cost-competitive and net-zero waste via advanced thermo-chemical conversion technologies is an promising solution to produce intermediates toward high value-added products [1–4]. Biogenic waste and residues are an attractive alternative to fossil fuels since they are not in competition with other utilization routes. One of the most favorable technologies is entrained-flow gasification, which will play a vital role in order to provide high-quality and tar-free synthesis gas. Follow-up products can be C_1-building blocks like methanol, higher alcohols, olefins (MTO) and liquid fuels like dimethyl ether (DME), gasoline (MtG) or sustainable aviation fuels (SAF). [5–8].

High-pressure and high-temperature gasification allows for almost complete feedstock conversion at short residence times, which is especially attractive for industrial-scale synthesis gas facilities. In addition, pressurized systems benefit the thermodynamic equilibria of the subsequent catalytic synthesis and reduce specific investment costs by smaller operational units. However, entrained-flow gasification is a complex system and demands high standards for durable and reliable operation. Besides feedstock preparation into a conveyable powder, other aspects like slagging, refractory interaction, devolatilization, char conversion kinetics and reactivity development, as well as strong structural changes of the char are necessary to be understood [9–13]. In the latter case, the chemical and physical char structure heavily depends on the particle thermal history during devolatilization and gasification [14–16]. Here, severe heat treatment leads to annealing-induced

* Corresponding author.
E-mail address: weiss.naim@tum.de (W. Naim).

https://doi.org/10.1016/j.fuel.2024.133848
Received 11 February 2024; Received in revised form 9 October 2024; Accepted 21 November 2024
Available online 28 November 2024

transformation of the carbonaceous matter into graphene-like structures. As a consequence, chars show lower reactivities. To achieve quantitive conversion, higher gasifying temperatures are necessary by O_2 input and thus the cold gas efficiency is lowered [17–21]. Therefore, annealing is of great importance in entrained-flow gasification [22].

In general, the influence of the thermal history on the char reactivity is widely investigated for various feedstocks and gasification technologies [22,23]. In particular under entrained-flow conditions, the devolatilization step has to be carried out under high heating rates in the range of 10^5 K s^{-1}, high temperatures above 1200 °C and short residence times up to 3 s [24–27]. For accurate reactivity determination, representative pyrolysis chars are necessary to be prepared under conditions similar to entrained-flow gasification [19]. Hence, the experimental set-up (e.g. wire-mesh, heat-strip, single-particle or drop-tube reactor) should fulfil these specific requirements for char preparation. Herein, the peak temperature, the heating rate, the residence time, but also the pressure show a great influence on resulting char reactivity [28].

Pyrolysis temperature dependency of the char reactivity is studied extensively [29–37]. For example, Senneca et al. [33] investigated the effect of the pyrolysis temperature from 900-1400 °C on the char reactivity and observed a decrease of CO_2 reactivity by a factor of 3. Peralta et al. [36] performed pyrolysis experiments in the range of 1000–2000 °C and detected that the O_2 reactivity almost halved. In general, decreasing reactivities with higher peak temperatures is widely reported and there is a broad consent toward its influence. Besides the more obvious consequences like char yield or annealing kinetics, also overlooked effects like surface oxygen complexes hindering the carbon rearrangement, phase transformation or the loss of catalytically active mineral matter can occur [38].

Another main focus is the influence of the heating rate. Cai et al. [39] investigated the effect of different rates in the range of 1–5000 K s^{-1} in a wired-mesh reactor at 1000 °C peak temperature and 2 s holding time. Char reactivity increased strongly from 1-100 K s^{-1} and reached a plateau at 1000 K s^{-1}. Higher heating rates of $4 \bullet 10^5$ K s^{-1}, closer to entrained-flow conditions, also lead to higher reactivities [40,41]. Such conditions are considered to promote structural carbon defects which not only leads to an increase of surface area, but also to a more reactive surfaces with a more widely distributed activation energy for both gasification and annealing.

The effect of residence time is strongly linked to the heating rate and peak temperature [34,42–45]. For example, Salatino et al. [34] studied the coal-derived char reactivity in a heat-strip reactor at high heating rates (10^6 K min^{-1}) and at temperatures up to 2000 °C in a time-scale of 0.2 s to 30 min. The results suggested that conversion rates decrease and char ignition shifts towards higher temperatures with longer holding times due to growth of graphitic structures. Mahapatra et al. [44] investigated the effect between 4.9–11.8 s at temperatures up to 1400 °C and demonstrated that the same trend also applies for drop-tube derived chars. At more characteristic residence times and temperatures for entrained-flow gasification, Feng et al. [45] and Netter et al. [42] made similar observations.

It is further reported that the effect of pressure rather influences the pore structure and morphology than the intrinsic char reactivity [46–51]. Moreover, it remains unclear if physical char properties fall in the scope of thermal annealing at all. Since in most cases the char reactivity is determined in a chemically-controlled regime at low temperatures, no influence of pyrolysis pressure on the intrinsic reactivity should be observed as demonstrated by Benfell et al. [51]. However, char morphology shows major relevance in high-temperature gasification in pore diffusion-controlled regime making surface area, porosity and pore size distribution analysis highly necessary information.

Also, various ash components influence the char reactivity [52–57]. For example, Pflieger et al. [57] found that mixing biomass-derived char with different minerals like K_2CO_3, $NaCO_3$, Fe_2O_3, CaO and MgO reduces the apparent activation energy in O_2, CO_2 and H_2O gasification reactions, especially for minerals containing K and Na. In contrast, Zolin et al. [58] studied the effect of leaching and demineralizing. They observed lower reactivities, especially at higher annealing temperatures. When ash components remained, the higher char reactivities are attributed to highly dispersed potassium on the char surface. Schneider et al. [37] noted similar phenomena by investigating char reactivity in secondary pyrolysis, prepared in the range of 1000–1600 °C under drop-tube conditions. They observed the highest char reactivity at 1600 °C pyrolysis temperature justified by high calcium dispersion despite severe graphitization. However, depending on the origin and pyrolysis conditions of the char, the catalytic potential is heavily dependent on the ash composition, melting temperature, devolatilization of mineral matter and also char sampling method [38].

In summary, char reactivity is strongly linked to its fuel precursor, pyrolysis set-up and preparation conditions. Further, the char preparation method directly influences the char structure and the morphology as well as nature of the inorganic mineral matter. For example, the deterioration of char reactivity is mostly explained by the loss of functional groups and reactive carbon sites as well as graphitization and the loss of catalytically active mineral matter. To uncover the structural behavior several characterization techniques like X-ray diffraction (XRD), Raman spectroscopy, Fourier-Transform Infrared-Spectroscopy (FT-IR), nuclear magnetic resonance spectroscopy (NMR), transmission electron microscopy (TEM), scanning electron microscopy with energy dispersive X-ray spectroscopy (SEM-EDX), sorption-techniques, but also *in-situ* methods like small-angle X-ray scattering (SAXS) and many more were applied [37,40,59–66]. Char characterization provides deep insights on structural information e.g. carbon structure, aromaticity, pore structure, soot formation, alkali dispersion and much more. This represents valuable information at microscopic particle level for a profound understanding of the conversion behavior for gasifier manufacturer and operators [67].

At reactor-scale however, experiment-based thermal annealing submodels for computational fluid dynamics (CFD) simulation are highly needed in the design and up-scaling of a gasifier [19,20,26,68]. For example, Tremel et al. [17] developed a char deactivation model, based on the generic assumption that the transformation of reactive into deactivated sites follow a simple Arrhenius type equation, where mainly the pre-exponential factor is affected. The feedstock-independent model shows very good agreement for various coals like anthracite, bituminous coal and lignite [30], but needs to verified for biogenic feedstocks. Senneca et al. [69] investigated the suitability of a deactivation model, formerly developed for coal, in the annealing of lignocellulosic biomass. Herein, several heat treatment experiments over a range of 273–1727 °C, 0.1–10^5 K s^{-1} and 0.02–20 000 s were conducted. They found that biomass follows the same deactivation kinetics as coal. In addition, Holland et al. [38] concluded that coal thermal annealing models could be in principle applied for biomass, however the deactivation mechanism seems to be much more complex due the heterogeneous nature of biomass. Here, complementary and in-depth char characterization could become more meaningful than before to support thermal annealing kinetic models.

Although many publications are reported to prepare chars in drop-tube reactors up to 1400 °C from different fossil and renewable feedstocks, just a few experiments are reported to carry out annealing experiments at even higher temperatures around 1600 °C and short residence times from 0.2-3 s [17,27,30,37]. Moreover, it is rather unclear how biomass-derived drop-tube chars evolve in their reactivity and structure under these harsh conditions.

To the best of our knowledge, there is no report on the relationship between char structure, reactivity and modelling parameters in the context of thermal annealing of biogenic residues like solid digestate at serious heat treatment of 1600 °C. Thus, we report on an analysis of the deactivation behavior of solid digestate by the investigation of pyrolysis char structure and reactivity modelling (Fig. 1). First, biomass chars are prepared in a pressurized entrained-flow reactor and subsequently characterized each in their reactivity in the presence of O_2 and CO_2. As

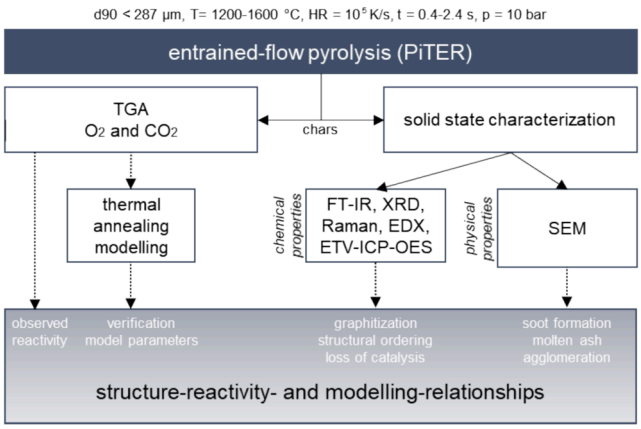

Fig. 1. Outline and experimental procedure of presented work.

suggested by Holland et al. [38], the experimental data are fitted to a deactivation model, formerly developed for coal [17], verifying whether the model can also represent the deactivation behavior of biogenic residues. In order to establish corresponding structure–reactivity and modelling-relationships the chars are investigated by FT-IR, XRD, Raman, SEM-EDX and ETV-ICP-OES.

2. Materials and methods

2.1. Fuel preparation and characterization

Solid digestate from a corn-fed biogas plant in Saxony, Germany is provided as granulate by VER Verfahrensingenieure GmbH. The granulate is further prepared to a pulverized fuel by pre-milling and fine-milling using a Retsch SM500 and Retsch SRM100 respectively. The powder is sieved at 250 µm. The resulting particle size distribution is measured by Laser Diffraction using Shimadzu, SALD-2201 (Fig. 2). The results show 90 % of the particles are smaller than 287 µm with a median particle size of 120 µm. Since the typical particle size of entrained-flow gasification is lower than 500 µm, the obtained powder is suitable for entrained-flow experiments.

Standard proximate (DIN 51718, DIN 51719 and DIN51720) and ultimate (DIN 51732/733, DIN 51724–3) analysis were performed in order to gain information about the water, volatile and ash content as well as the elemental composition. Moreover, the heating value (DIN51900) and the ash oxide composition (DIN51730) were determined by X-ray fluorescence spectroscopy (XRF). The fuel analysis is summarized in Table 1. The results show a characteristic biomass fuel with relatively high ash content of 23.7 %, low fixed carbon of 15.4 % and high oxygen content of 55.1 %. The lower heating value of 15.1 MJ/kg further shows the potential of biogenic residues as suitable feedstocks. The ash composition with a high K_2O content (25.5 %) might enable catalytic activity, however the ash is also rich in SiO_2 (37.0 %) and P_2O_5 (14.4 %). The catalytic potential is quantified by the Alkali-Index AI (Eq. (1)). Compared to anthracite (< 10) and lignite (54.7), solid digestate (AI = 26.3) indicates a rather moderate influence on char reactivity [30,70].

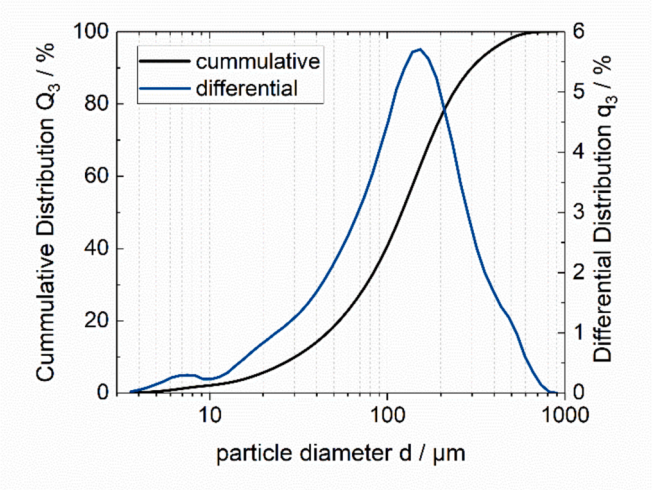

Fig. 2. Particle size distribution of prepared fuel measured by Laser Diffraction (Shimadzu, SALD-2201).

$$AI = w_{ash.rawfuel} \bullet \frac{Na_2O + K_2O + CaO + MgO + Fe_2O_3}{SiO_2 + Al_2O_3} \quad (1)$$

2.2. High-pressure high-temperature entrained-flow reactor (PiTER)

Pyrolysis chars were prepared at temperatures of 1200 °C, 1400 °C and 1600 °C and at residence times up to 2.4 s at 10 bars in an entrained-flow reactor (PiTER). The experimental set-up is shown in Fig. 3 and is described in more detail in our previous work [27,42]. In brief, the 7.12 m high reactor is an electrically-heated entrained-flow reactor (1800 °C and 50 bar). The reaction gas can be a mixture of Ar/N_2, O_2, CO_2, H_2O, H_2 and CO. Besides gasification experiments, also pyrolysis experiments can be carried out. The reactor consists of a pre-heating and a reaction zone (d_i = 70 mm, L = 2200 mm). A vibrating dosing unit with a Ar/N_2 carrier gas feeds a pulverized fuel up to 5 kg h^{-1} to the reaction zone, where high heating rates of 10^4-10^5 K s^{-1} are modelled [17,26]. Char samples were derived by a high-adjustable oil-cooled sampler at different averaged particle residence times up to 3 s. Uncertainties are considered by correction of the gas residence time by the influence of particle free fall velocity, the radial velocity distribution within the reaction tube and by the produced gas amount as a consequence of devolatilization. The product gas is cooled by a water quench at the bottom of the reactor and the gas composition (O_2, CO_2, CO, H_2, CH_4) is analyzed online by SICK, GMS 320/310.

2.3. Thermogravimetric analyzer (TGA)

A thermogravimetric analyzer TGA STA-1700 by Linseis GmbH is applied to determine the reactivity of entrained-flow chars derived by

Table 1
Fuel properties of solid digestate (ar = as-received, wf = water free, daf = dry and ash free).

Proximate analysis		
water	10.2	wt.-% (ar)
volatiles	50.7	wt.-% (wf)
fixed carbon (by difference)	15.4	wt.-% (wf)
ash (815 °C)	23.7	wt.-% (wf)
Ultimate analysis		
C	56.7	wt.-% (daf)
H	7.3	wt.-% (daf)
O (by difference)	32.1	wt.-% (daf)
N	3.6	wt.-% (daf)
S	0.3	wt.-% (daf)
Heating value		
LHV	16.8	MJ/kg (wf)
Normalized ash composition (XRF)		
SiO_2	37.0	wt.-% (wf)
Al_2O_3	1.6	wt.-% (wf)
CaO	7.8	wt.-% (wf)
Fe_2O_3	1.5	wt.-% (wf)
SO_3	4.2	wt.-% (wf)
MgO	5.5	wt.-% (wf)
Na_2O	2.4	wt.-% (wf)
K_2O	25.5	wt.-% (wf)
MnO	0.2	wt.-% (wf)
P_2O_5	14.4	wt.-% (wf)

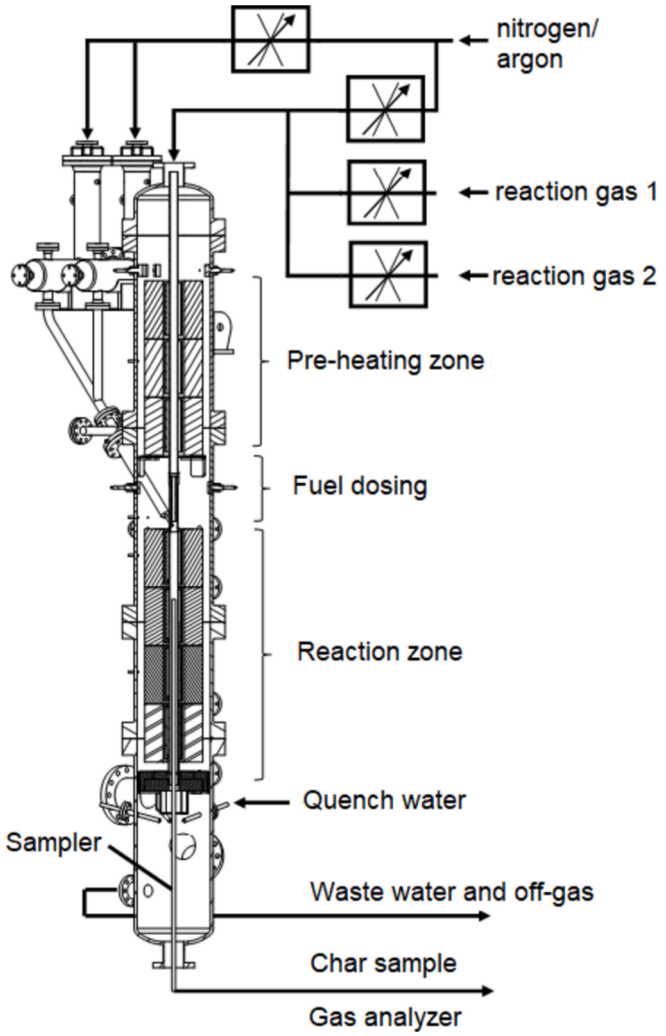

Fig. 3. Pressurized High-Temperature Entrained-Flow Reactor (PiTER) is applied for pyrolysis char preparation and gasification experiments of pulverized fuels [30].

PiTER. Herein, 10 mg of char dust are introduced in a ceramic crucible so that the lowest possible height of the bulk is achieved. The particle size of char samples is much lower than the raw fuel due to fragmentation during pyrolysis promoted by the high volatile content of 50.7 %. The weight change and the temperature of the sample are recorded continuously. Prior to reactivity measurements, heating-rate experiments at 5 K min^{-1} in O_2, 25 % synthetic air (5 % O_2) in N_2 and in CO_2, 50 % CO_2 in N_2 were conducted in order to determine reaction temperature (SI, Fig. 1). In order to avoid mass transport limitations, isothermal reaction temperature in O_2– and CO_2-experiments are set as low as possible to 350 °C and 725 °C respectively. This is further promoted by the very small char particles and sample preparation method. First, the analyzer is heated up to the set temperature in 200 ml min^{-1} N_2 and at steady-state conditions the gasifying agent is introduced. The volume flow rate is set to 50 ml min^{-1} synthetic air, 150 ml min^{-1} N_2, 100 ml min^{-1} CO_2 and 100 ml min^{-1} N_2. Char conversion X(t) and observed reactivity r_{obs} were calculated from time-dependent mass signal change according to Eq. (2) and Eq. (3).

$$X(t) = \frac{m_0 - m(t)}{m_0} \tag{2}$$

$$r_{obs} = -\frac{1}{m(t)} \bullet \frac{dm}{dt} = \frac{1}{1 - X(t)} \bullet \frac{dX}{dt} \tag{3}$$

$$r_{intrin} = r_{obs}|_{X=0.05}^{X=0.20} \bullet \frac{1}{S} \tag{4}$$

The initial observed conversion rate r_{obs} is chosen to be defined as average between char conversion X = 5–20 % (Eq. (4)). Above 5 %, errors from the gas change were minimized and below 20 % only minor changes of the structural char properties were reasonable assumed.

2.4. Modelling thermal deactivation

In literature, the deterioration of char reactivity is mostly explained by loss of functional groups and active carbon sites, the graphitization of the carbon structure and the loss of catalytic active mineral matter. The feedstock-independent modelling approach in this work, developed by Tremel et al. [17], is based on an overall reactivity and therefore doesn't distinguish between these different structural deactivation mechanisms. However, theoretical approaches were made. In brief, two different active sites are assumed, with fresh sites r_{fresh}, which are very reactive and with deactivated sites r_{deact}, that are much less reactive. Herein, the reactivity is the sum of fresh r_{fresh} and deactivated sites r_{deact}. The transformation to deactivated sites is caused by the heat treatment severity, which is temperature and time dependent and described by an Arrhenius type equation. It is assumed that thermal deactivation only affects pre-exponential factor k_0 with A_{max} as the ratio of the pre-exponential factors $k_{0,fresh}$ of a fresh char and $k_{0,deact}$ of a maximum deactivated char. Hence, the following simplified Eq. (5) and Eq. (6) were derived [17]:

$$A_i = 1 + exp[-F_0 \bullet exp(\frac{-E_A}{R \bullet T}) \bullet t] \bullet (A_{max} - 1) \tag{5}$$

$$A_{max} = \frac{r_{max}}{r_{min}} = \frac{k_{0,fresh}}{k_{0,deact}} \tag{6}$$

The deactivation model is fitted to experimental data by the least square method resulting in the relative reactivity A_i and in the model parameters A_{max}, the pre-exponential factor F_0 and the activation energy E_A. At 0 s residence time, A_{max} is defined as a theoretical value describing initial reactivity independently from the char thermal history and calculated by least square method. In several publications a good correlation is previously demonstrated for mainly fossil fuels between experimental data and model [17,27,42]. Since the theoretical approach could be also applied for bio-chars the model was used to check whether a good agreement could be also found for biomass.

2.5. Char characterization

2.5.1. Fourier-Transform Infrared-Spectroscopy (FT-IR)

To identify functional groups, the char samples were analyzed via Fourier-transform infrared-spectroscopy (FT-IR) using a Varian FT-660 IR spectrometer (Agilent Technologies). For this purpose, the samples were pressed into pellets with potassium bromide KBr and measured in transmission in the range of 400–4000 cm^{-1} in ambient air. A KBr pellet was used as reference material for the background subtraction and the resulting spectra were normalized to eliminate pellet thickness.

2.5.2. X-ray diffraction (XRD)

Crystalline phases of the chars were examined using X-ray powder diffraction (XRD). The measurements were carried out on an X'pert PRO XRD diffractometer (PANalytical). The measurement was carried out in ambient air with Cu-K-α radiation (Cu-K-α1 = 1.5406 Å, Cu-K-α2 = 1.5444 Å) at angles of 5-80° with a step size of 0.017° with a measurement time of 30 min with a data acquisition time of 0.51 s. In the obtained diffractograms, the background and the Cu-K-α radiation were subtracted and then smoothed.

2.5.3. Raman spectroscopy

Raman spectroscopy in the range of 90–3450 cm^{-1} was performed with an inVia Raman spectrometer (Renishaw) equipped with a He-Ne laser (633 nm, ~17 mW at the source) and an optical microscope (Leica). The samples were slightly pressed to obtain a flat surface prior to data acquisition. 5 positions were probed 20 times to give reasonable average information of the sample (1 % laser intensity, 60 s acquisition time, 2.400 lines mm^{-1} grating, spectral range of 60–1300 cm^{-1}). Data treatment (cosmic ray removal, noise filtering, truncation, baseline subtraction and averaging) was done with the software WiRE 4.4 (Renishaw). The spectra were normalized to the D band.

2.5.4. Scanning electron microscopy coupled with energy-dispersive X-ray analysis (SEM-EDX)

SEM analysis (Fig. 11) were performed in the RWE laboratory with a Zeiss Evo MA 25 including an Everhart-Thornley secondary electron detector and an EDX detector (Oxford XMAX-50) with 15 kV acceleration voltage for element mapping (SI, Figs. 4 and 5).

SEM images (Fig. 12) were recorded at KIT with a LEO Gemini 982 from Zeiss (Oberkochen, Germany) equipped with an annular high brightness in-lens-SE detector for high resolution and true surface imaging. A laterally mounted SE detector (Everhart-Thornley-type) provides topographical contrast (sensitive for SE + BSE). The beam accelerating voltage was 10 kV. The determination of the chemical

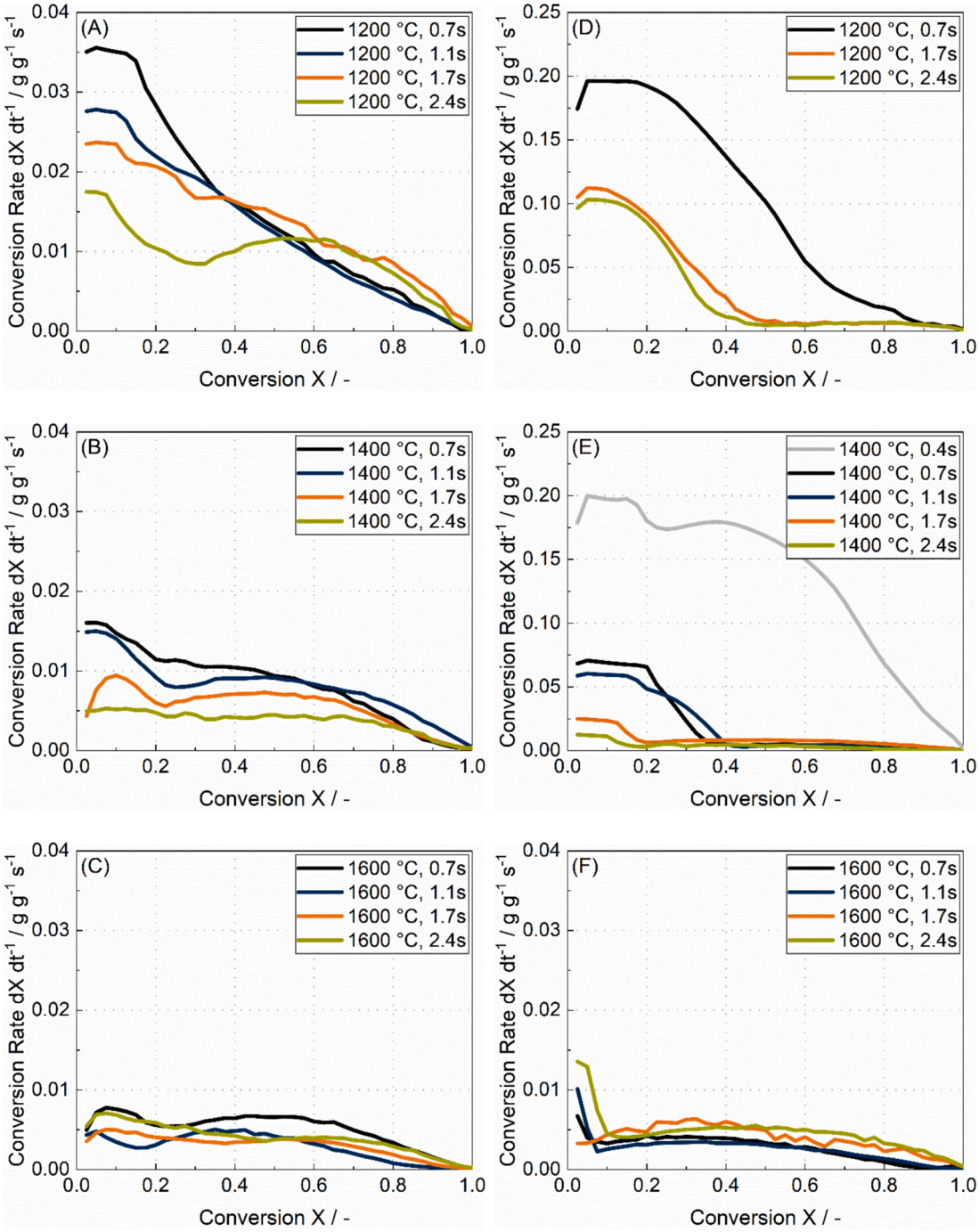

Fig. 4. Gasification conversion rate dX dt^{-1} of pyrolysis char samples (10 mg), isothermally in a TGA (A, B, C) 350 °C, 25 % synthetic air in N_2, (D, E, F) 725 °C, 50 % CO_2 in N_2.

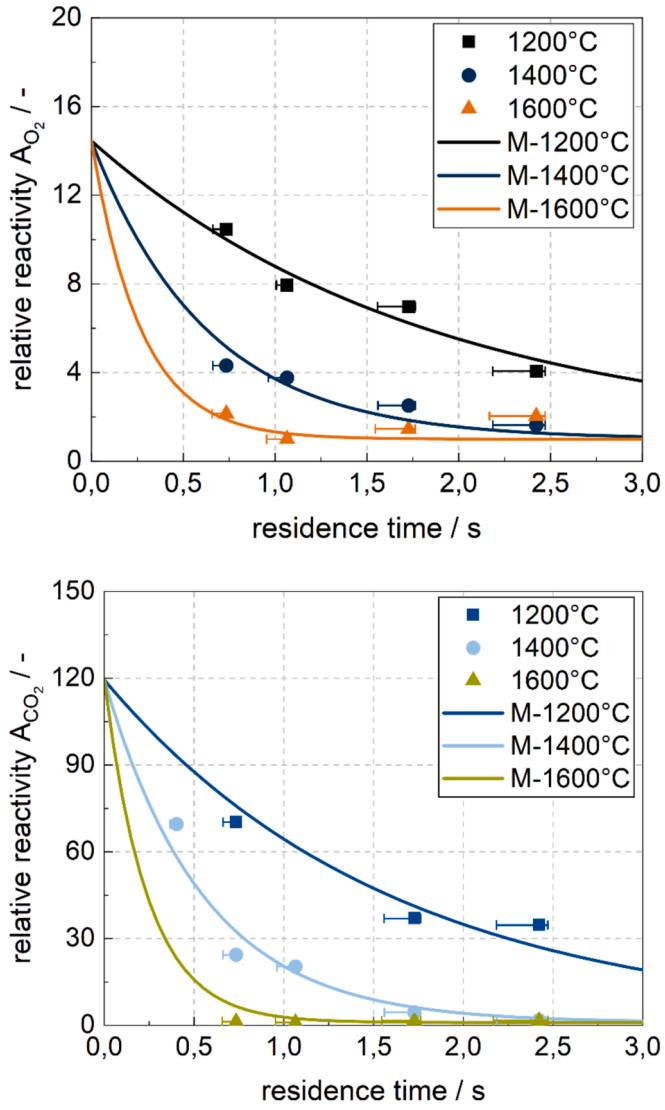

Fig. 5. Experimental and modelled relative char reactivity A_i in (top) O_2 and (bottom) CO_2 as a function of pyrolysis temperature and residence time.

composition (Table 3 and SI, Fig. 6) was performed using an Oxford INCA Penta FETx3 EDX system (Abingdon, UK).

2.5.5. Electro-thermal evaporation with inductively coupled plasma optical emission spectrometry (ETV-ICP-OES)

The concentration of ash elements of prepared chars, in particular of potassium K, chlorine Cl and phosphorus P, were determined by electro-thermal evaporation connected to an inductively coupled plasma optical emission spectrometry (ETV-ICP-OES). The set-up is validated to other elemental analysis techniques and is described elsewhere in more detail [71].

3. Results and discussion

3.1. Char conversion rates

The thermal history plays a major role in char gasification reactivity. Thus, chars were prepared under various entrained-flow conditions and subsequently characterized towards their O_2– and CO_2-reactivity in a TGA (Fig. 4).

Among all temperatures and residence times, the highest conversion rates are observed at the lowest pyrolysis temperature of 1200 °C.

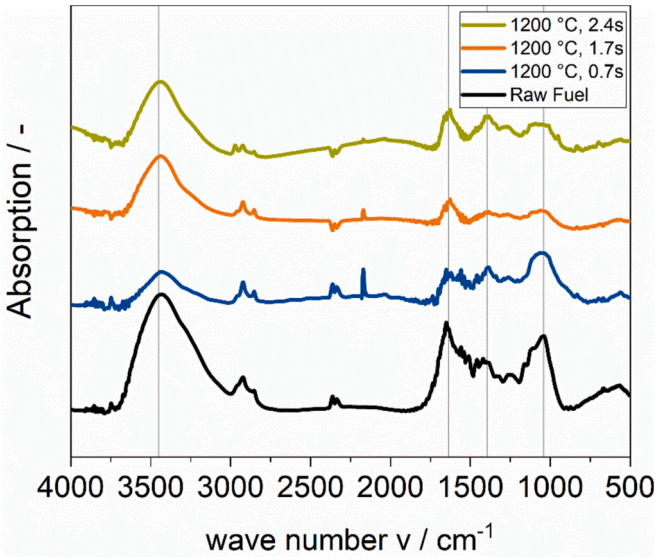

Fig. 6. FT-IR spectra of the raw fuel and the entrained-flow pyrolysis chars show loss of functional groups with longer residence times at 1200 °C.

However, conversion rates deteriorate rapidly when the pyrolysis temperature is increased from 1200 °C to 1400 °C. At 1600 °C all chars show comparable conversion rates independently from gasifying agent suspecting that chars undergo severe structural changes. Up to 1400 °C, a noticeable decrease of conversion rates with longer residence times is showed. The biggest effect is observed in CO_2 reaction at 1400 °C. Especially, the conversion rate at 1400 °C and 0.4 s appears to be similar to that rate at 1200 °C and 0.7 s. However, the influence of residence time diminishes almost completely, when pyrolysis temperature was increased to 1600 °C, suggesting that peak temperature shows a much greater consequence on char structure than the residence time. Yet, in CO_2 atmosphere the impact of pyrolysis conditions is considerable stronger. Below $X = 0.25$ the level of conversion rates is highly impacted by the pyrolysis conditions [53]. At conditions of 1200 °C, 2.4 s a slight increase of conversion rate in O_2 is noted at $X = 0.3$, which could have many reasons like different kind of carbon actives sites, the accessibility of blocked pores filled with molten ash, or catalytic active sites and many other. This is similarly found at 1400 °C at shorter residence times, however the effect seems to be less pronounced. In contrast, the conversion rates align above $X = 0.5$. Interestingly, the level of the conversion rate shows two distinct stages below and above $X = 0.5$, which could indicate different annealing-induced carbon structures [72]. These results are in line with literature, where a decline of char reactivity with increasing severity of heat-treatment, in particular, peak temperature and holding time is stated for wide range of fuels [31,35,37].

3.2. Relative reactivity and deactivation modelling

In general, it should be distinguished between an intrinsic reactivity loss due to a lowered surface area or a loss of active sites due to the formation of ordered and planar carbon structures (Eq.(4)). While char morphology gives explanations about the surface area, distribution of micro-, meso- und macro pores as well the blocking and closing of pores due to ash melting, the chemical structure of carbon has to be investigated specifically. The surface area does play a role in char reactivity with regard to the number of active sites, however the nature of active sites seems to have a greater influence on the intrinsic reactivity r_{intrin} [30]. Consequently, the initial conversion rates were stated to the observed reactivities r_{obs}, emphasizing on the chemical char structure. Initial conversion rates are averaged between $X = 0.05$–0.2 and fitted to the deactivation model [17]. The results are shown in Fig. 5 and Table 2.

Table 2
Fuel-specific model parameters of thermal annealing for solid digestate chars.

gasifying agent	O_2	CO_2
R^2	0.92	0.97
A_{max} / –	14.45	119.44
F_0 / s^{-1}	4366.17	4488.55
E_A / kJmol^{-1}	110.08	108.75

Table 3
Specific concentration of K and P on char-surface by EDX and in char-ash by ETV-ICP-OES.

	EDX / wt.-%			ETV-ICP-OES / g kg^{-1}		
char sample	K	Cl	P	K	Cl	P
1200 °C, 2.4 s	13.7	6.1	0.5	95.4	59.4	27.6
1400 °C, 2.4 s	15.2	6.0	2.3	134.2	82.7	56.1
1600 °C, 2.4 s	18.1	5.3	2.7	162.3	88.4	68.9

According to Eq. (6), relative reactivity A_i describes the reactivity ratio of the actual char (subscribed by i) to the most deactivated char as a function of temperature and residence time. In O_2 atmosphere, the most reactive char at 1200 °C and 0.7 s is 10.5 times faster than the slowest char at 1600 °C and 1.1 s. With increasing residence time, A_{O2} drops to 4.1. At 1400 °C, the reactivity decreases from 4.3 to 1.6. Chars prepared at 1600 °C, show an initial decrease from 2.2 to 1, but with longer residence times a slight increase in reactivity to 1.5 and up to 2.0 is observed. Yet, the slight increase could be a consequent of the mass signal-to-background noise accuracies since the conversion rates of the samples seem to be rather similar.

However, the degree of deactivation seems to be stronger for CO_2 char reaction. The most reactive char at 1200 °C, 0.7 s shows a relative reactivity A_{CO2} of 70.3 and decreases to 34.7 at 2.4 s. With further increase in pyrolysis temperature, the deactivation is even more pronounced from 69.6 at 0.4 s down to 1.8 at 2.4 s, suggesting a stronger structure dependency for CO_2 reactivity. Compared to O_2 reactivity at 1600 °C, a considerable increase in reactivity with longer residence times was not observed.

These results indicate thermal annealing impacts CO_2 and O_2 reactivities potentially in different manner. Since both, carbon active sites and CO_2 have to be activated at given reaction temperature, the carbon structure is much more sensitive toward CO_2. In contrast, O_2 is a strong oxidant, so that the conversion could undergo different reaction pathways during annealing. Similar behavior was previously observed for bituminous coals and petroleum coke by Senneca et al. [72].

The deactivation model was applied (Eq. (5) and (6)), predicting the measured reactivity data quite well ($R^2 > 0.92$). These data confirm that biomass follows similar deactivation kinetics as coal as previously reported by Senneca et al. [69]. The parameters $A_{max,O2}$ and $A_{max,CO2}$ were fitted to obtain values of 14.45 and 119.44 respectively, which can be interpreted as theoretical initial reactivity. Moreover, rather similar pre-exponential factors F_0 (influence of pyrolysis residence time) and activation energies E_A (influence of pyrolysis temperature) in Table 2 for both atmospheres suggests that O_2 and CO_2 reactions undergo similar deactivation kinetics. However, the exception seems to be A_{max}, which is very much different for O_2 and CO_2, indicating that annealing seems to have a greater influence on A_{max} than E_A and F_0 for solid digestate. Higher reactivities of fresh chars shortly after devolatilization around 0.2 s are modelled. It displays the necessity for preparing chars at residence times below 0.4 s to further validate the model prediction. At the same time, it is concluded that chars undergo strong structural changes within the first milliseconds just after devolatilization around 0.2 s [26,38].

Although applied model was formerly developed for coal, the theoretical approach of the ratio between reactive and deactivated actives sites was successfully verified for bio-chars. However, the deactivation mechanism and the nature of the active sites still remains unclear. Therefore, several char characterization techniques are applied to reveal the structural states during entrained-flow gasification.

3.3. The influence of pyrolysis temperature and residence time on char structure

3.3.1. Infrared spectroscopy

To detect the loss of functional groups during pyrolysis, the raw fuel and the char samples were analyzed via FT-IR (Fig. 6). At 1200 °C, a loss of C=O functional group at 1042 cm^{-1} is observed due the decomposition, especially at 1.7 s and 2.4 s [73]. Additionally, more functionalities at 1396 cm^{-1} related to aliphatic C–H structures disappear with longer residence time at 1.7 s, but seem to form again at 2.4 s, which cannot be explained [74]. A more pronounced band at 1620 cm^{-1} at 2.4 s is detected, which corresponds to polyaromatic C=C stretching [21]. Stretching vibrations of aliphatic hydrocarbons can be observed between 2860–3000 cm^{-1}, which change with structure at higher residence time of 2.4 s [75]. Further, hydrogen-bonded O–H stretch at around 3450 cm^{-1} can be observed for all samples and it appears less pronounced for 0.7 s residence time. This can be interpreted as the water capacity of the char [76]. No changes are observed with higher pyrolysis temperatures. Yet, char reactivities at 1400 °C and 1600 °C suggesting severe structural changes. These changes could not be elucidated using FT-IR making further characterization necessary.

3.3.2. X-ray diffraction (XRD)

One of the reasons leading to different reactivities might be in the crystalline carbon structure [29,32]. Hence, the char samples were analyzed by XRD to check if crystalline carbon can be found (Fig. 7). The formation of crystalline phases plays a major role for ash melting, refractory corrosion and slag viscosity behavior in entrained-flow gasification [77]. Though, the scope of this work emphasizes on the thermal annealing and consequently the discussion is focused towards the carbonaceous matrix ordering. Two scattered carbon reflections are of special interest. One reflection emerges at 24-25° (0 0 2), which corresponds to ordered and stacked graphene-like layers while the second reflection at 44-45° (1 0 0) suggests layered aromatic ring structures [21,37,48].

No characteristic reflections are found in the char samples up to 1400 °C. Carbonaceous reflections at 24-25° start to appear at 1600 °C and 0.7 s. If the residence time is further increased, the reflections at 24-25° narrow and intensify suggesting the formation of polycrystalline structures. In addition, the presence of aromatic ring structures was suggested by weak reflections at 45.2°, however the reflection seemed to be slightly shifted. These results show that the degree of graphitization might increase when peak temperature and residence times are amplified. This could explain the strong reactivity drop from $A_{max,CO2}$ 70.3 down to 1.3, that could be due to the formation of stacked graphene-like layers in the char at 1600 °C.

However, the interpretation of the carbon scattering appears limited since the intensity of the reflections are quite weak, when compared to other studies [29,32]. Several other distinct reflections of ash forming components are found with high intensity, which effect the carbon scattering during the measurement. This is further promoted by the enriched ash content of the chars up to 63 % (1600 °C, 1.7 s) and low fixed-carbon content (15.4 %) of the feedstock (Table 1). Another reason for the weak carbon reflections is the heterogeneous elemental nature of the feedstock. The process of crystal formation might be inhibited by heteroatoms like H, N, O and S. While in other studies [29,32] the carbon content is greater than 90 % and therefore the concentrations of heteroatoms are relatively low, strong crystalline structures were observed at 24-25°, the opposite behavior was found in this work. Hence, heteroatoms could prevent carbon crystal formation during annealing of biomass. XRD patterns did not significantly change between the samples treated at 1200 °C and 1400 °C, indicating that the

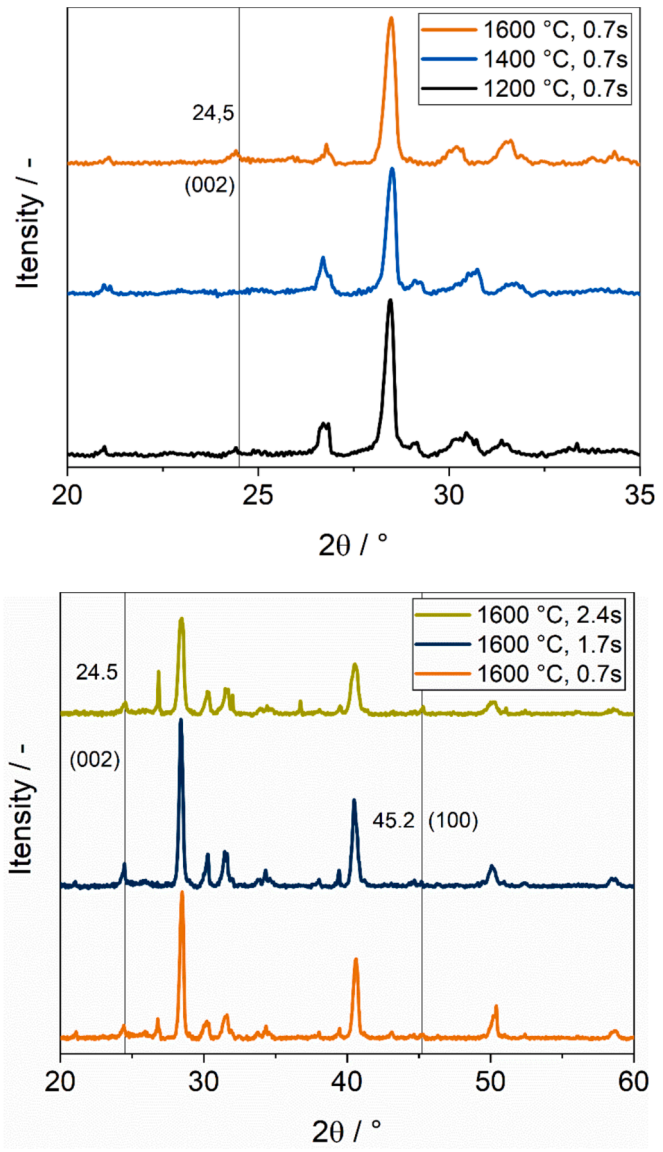

Fig. 7. XRD reflections of entrained-flow pyrolysis chars. (top) Influence of temperature on reflections at residence time of 0.7 s (bottom) Influence of residence time at 1600 °C.

change in activity is of a different nature than phase changes. Hence, other characterization methods are necessary.

3.3.3. Raman spectroscopy

Carbon structure and graphitization were further uncovered by Raman spectroscopy. All normalized spectra were of similar shape and show two bands at around 1340 cm^{-1} and 1600 cm^{-1}, which correspond to amorphous sp^3-hybridized (D band) and crystalline graphene/graphite-like sp^2-hybridized structures (G band) respectively (Fig. 8). The valley V at around 1487 cm^{-1} suggest the formation of partly-amorphous and partly-crystalline structures that are stopped in their annealing-induced crystallization process probably by hetero atoms [21,28,35,43,67]. The presence of these peaks with different intensities clearly indicates the formation of graphite domains, which can be interpreted that independently from pyrolysis conditions a mixture of amorphous and ordered structures are found in all chars. However, the shoulder between 1100–1300 cm^{-1} becomes sharper with higher pyrolysis temperatures. Same behavior is also observed at longer residence times at 2.4 s. No discernable Raman peaks were observed for the raw biomass.

To compare the char samples relatively to each other in a more reliable manner, Sadezsky et al. [66] proposed a deconvolution of the two peaks at 1340 cm^{-1} and 1600 cm^{-1} into the D_1, D_2, D_3, D_4 and G band. The Raman spectrum for the char treated at 1600 °C for 0.7 s is shown in Fig. 9, also depicting the linear data fitting and deconvoluted peak regions.

Details of the peak fitting for deconvolution can be found in the SI, Table 1, Figs. 2 and 3. Deconvolution suggests the presence of the G band, indicating highly ordered graphite domains, the D_1 band, showing disordered graphitic lattice domains, the D_3 band, indicating amorphous carbon and to smaller degrees the D_4 band, representative for disordered graphitic lattice domains including polyenes or ionic impurities.

After deconvolution the full-width-half-maximum (FWHM) of the D_1 band is used as measure of the graphitization, with decreasing values demonstrating higher graphitization degrees [66]. Fig. 10 shows the change of the FWHM at constant residence time of 0.7 s with increasing temperatures as function of initial char conversion rates in CO_2 atmosphere. A steadily declining FWHM of the D_1 band could be detected indicating a pronounced graphitization while initial char conversion rates deteriorate with increasing pyrolysis temperature [37,66]. By comparison, FWHM values at constant temperatures no observable trend, suggesting that peak temperature exerts a more significant influence than residence time on the graphitization process under entrained-flow conditions. In addition, the shift in FWHM of the D_1 band might also underline the distinct two stages in CO_2 char reactivity in Fig. 4. Hence, the transformation of amorphous into growing aromatic

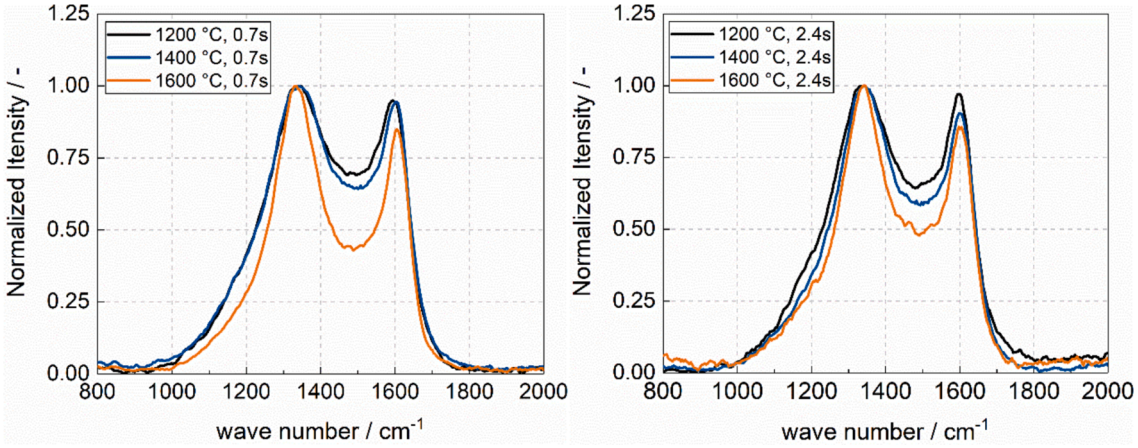

Fig. 8. Normalized Raman spectra of entrained-flow pyrolysis chars show the influence of temperature and residence time (left: 0.7 s, right: 2.4 s) on D and G band peaks.

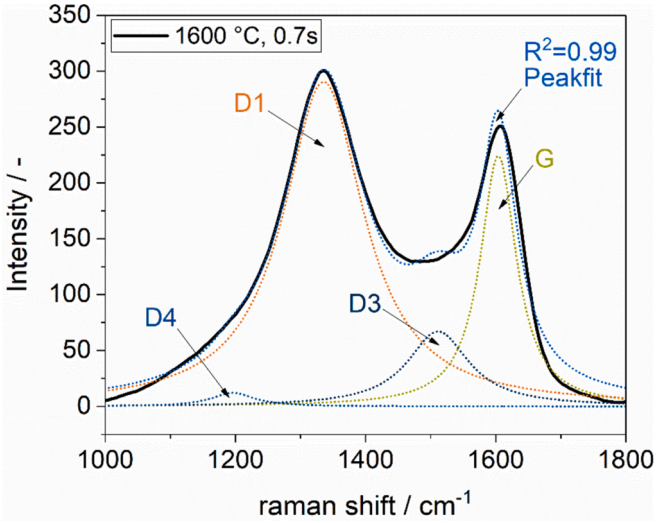

Fig. 9. Raman spectrum for pyrolysis char at 1600 °C for 0.7 s (black), including linear peak fit (light blue), deconvoluted peaks D_1 (orange), D_3 (dark blue), D_4 (mid blue) and G (green).

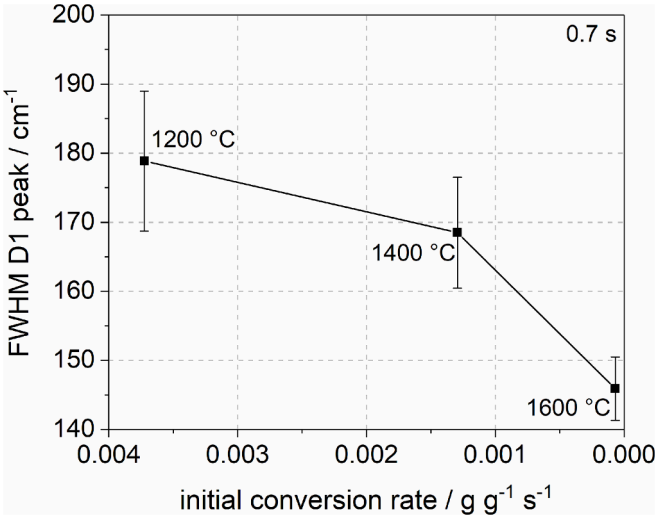

Fig. 10. FWHM of the D_1 band of chars treated at 1200 °C, 1400 °C and 1600 °C (0.7 s) as a function of initial conversion rates in CO_2 atmosphere. Error bars indicate the uncertainty originating from the peak fitting.

structures as well as the presence of graphite-like crystals is concluded.

3.3.4. SEM-EDX and ETV-ICP-OES

Prepared chars at 1200 °C and 1600 °C at 2.4 s were further investigated by SEM to show the effects on micro structure and morphology (Fig. 11). A char-covering ash layer is observed almost throughout the whole sample. More importantly, ordered structures were uncovered by SEM. EDX shows that ring structures are mainly oxygen and carbon atoms (SI, Fig. 4).

XRD results exclude such big crystals, since no reflections were found at 1200 °C. However, the Raman spectra suggests the existence of a mixture of ordered structures and amorphous carbon. Yet, the raw biomass does not show any graphitic-like structures in the Raman spectra due to missing heat-treatment. Therefore, we suspect a heterogeneously annealed sample where also some cellular structures could remain which could be attributed to observed structures. However, since pyrolysis kinetics are quite quick at these high temperatures and long residence times, the observed ring structures were referred to the

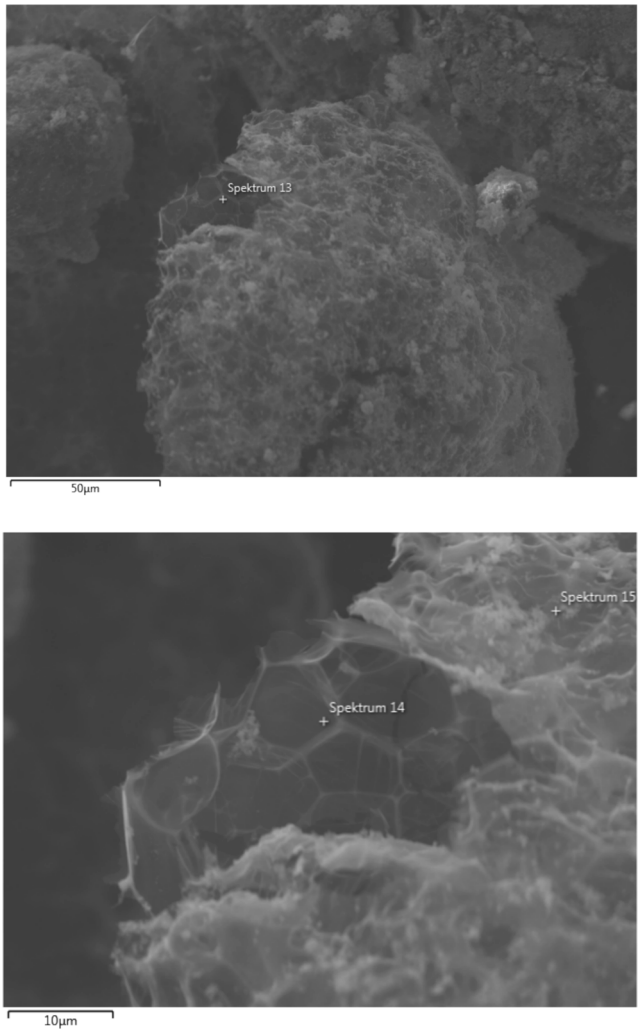

Fig. 11. Ordered char structure of entrained-flow pyrolysis char (1200 °C, 2.4 s), uncovered by SEM images in (top) 50 µm and (bottom) 10 µm resolution.

carbonaceous matrix as a consequence of high-temperature annealing. At 1600 °C these ordered structures could not be found due to the complete coverage with molten ash (SI, Fig. 5).

When higher resolution is applied (Fig. 12), the formation of typical cenospheres during pyrolysis at 1200 °C, 2.4 s were detected that are promoted by the high volatile content of the fuel (Table 1). In both samples the formation of soot is found. At 1200 °C, the soot seems to be distributed rather homogeneously with a uniform particle size (Fig. 12, left), while with higher temperatures, soot aggregation with a bigger particle size distribution is observed (Fig. 12, right). Yet, further methods like TEM or HRTEM are necessary for a more detailed analysis of the soot formation. An influence on char reactivity might be possible, but due to the highly ordered carbon structure of the soot, the ignition shifts towards higher temperatures compared to the measured char reactivity temperatures at 350 °C (O_2) and 725 °C (CO_2) [13]. Thus, it is concluded that the influence of soot on char reactivity is negligible and annealing-induced structural changes play a more dominant role.

Char deactivation might be promoted by the loss of catalytic active mineral matter. Although the ash composition shows moderate catalytic potential (AI = 26.3), the ash is also rich in P_2O_5 (14.4 %) that could inhibit the formation of active components (Table 1). Conversion rates at pyrolysis conditions of 1200 °C, 2.4 s show a slight increase between X = 0.3–0.5 that might show that different kind of pores open up during char conversion to catalytically actives sites (Fig. 4). Hence, ETV-ICP-OES is applied and EDX mapping (SI, Fig. 6) is performed for char-ash

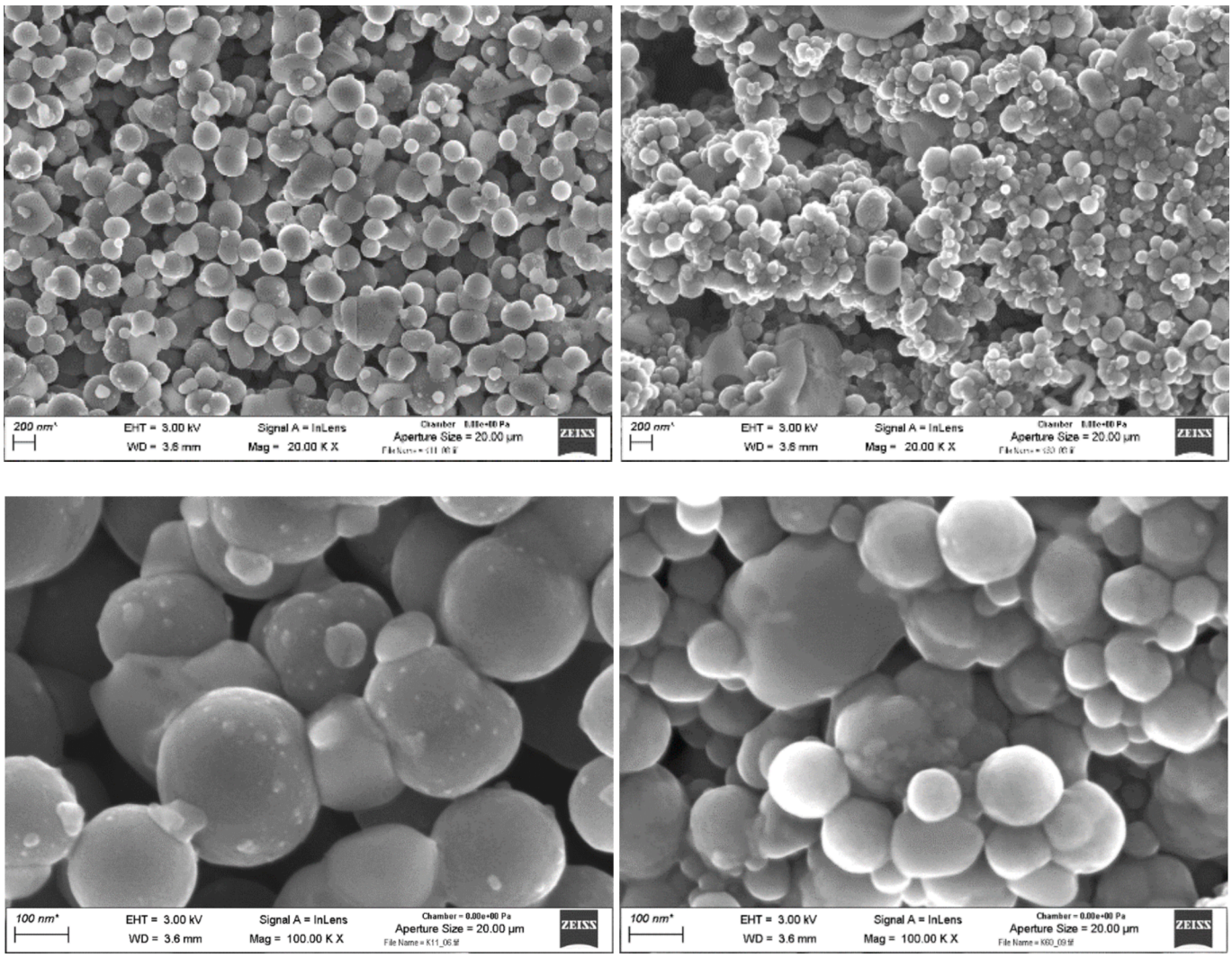

Fig. 12. SEM images in (top) 200 nm and (bottom) 100 nm resolution show soot agglomeration in entrained-flow pyrolysis chars, prepared at (left) 1200 °C, 2.4 s and (right) 1600 °C, 2.4 s.

analysis and to identify bulk concentration respectively (Table 3).

For K and P, the concentration is lower compared to raw ash composition (Table 1). That indicates a release and loss of mineral matter during devolatilization lowering the catalytic potential. In case of Cl, ETV shows increasing concentrations while EDX values decrease slightly. Hence, deposited aerosols like KCl are suspected to be found, which were initially released during the devolatilization process and subsequently condensed on the char due the sampling method [58,78]. However, increasing concentrations and a small degree of clustering of K and P with higher pyrolysis temperatures were found (Table 3 and SI). Also, the agglomeration and sintering of other ash forming elements like Si is identified. Therefore, the growing concentrations of K and P with higher pyrolysis temperatures could explain slightly higher char reactivities at 1600 °C, however the general influence seems to remain quite low due to loss of mineral matter and rather moderate catalytic potential of the raw fuel. Thus, the slight increase is more likely due to the mass signal-to-background noise accuracies. Compared to the loss of mineral matter, the strong carbon deactivation according FT-IR, XRD, Raman spectroscopy and SEM is concluded to be the more dominant mechanism.

In summary, char deactivation is explained by the most common mechanisms like loss of functional groups (FT-IR) and catalytic mineral matter (EDX, ETV-ICP-OES) as well as graphitization or growth of ordered crystalline structures (XRD, Raman spectroscopy, SEM). The analysis of chemical char structure explains the annealing-induced reactivity loss. The influence of physical char morphology has to be further investigated with other methods like Hg-porosimetry, TEM or HRTEM in order to depict a more precise char reactivity in pore diffusion-controlled regime.

Although the deactivation modelling approach can not differentiate between these mechanisms mathematically, there is a very good agreement with the experiments. Compared to the reactivity toward O_2, the results suggest a much stronger deactivation for CO_2, but the deactivation kinetics appeared to be rather similar. However, that seems to be still up for debate [38]. Hence, there is a need for more biogenic fuels to be investigated in their deactivation behavior to verify this observation, especially at relatively high temperatures around 1600 °C.

In general, these structure-based results which provide a dataset for model development at high temperatures massively help in accurate and reliable gasifier design. Presented results promote to establish a sustainable value-chain for the production of chemicals and liquid fuels via advanced gasification technologies by providing design parameters and a deep microscopic understanding of the conversion behavior.

4. Conclusions

Pyrolysis chars were prepared under pressurized entrained-flow conditions and characterized in their reactivity and structure as well

as in their fitting potential to deactivation model:

(1) In the char reactions toward O_2 and CO_2, pyrolysis conditions show a strong influence on reactivity with higher temperatures and longer residence times. The most reactive char is prepared at 1200 °C, 0.7 s while in contrary the most deactivated char results from conditions at 1600 °C, 1.1 s. Since O_2 ($A_{max,O2} = 14.45$) is a strong oxidant, carbon structure plays a much more important role toward CO_2 ($A_{max,CO2} = 119.44$) since both carbon active sites and gasifying agent have to be activated.
(2) Experimental data and deactivation model predictions are in good agreement and successfully verified for solid digestate chars. Further, rather similar F_0 and E_A indicate that O_2 and CO_2 reactions might undergo comparable deactivation mechanism. In addition, modelling suggests strong structure–reactivity dependency shortly after devolatilization. Accurate deactivation model ($R^2 > 0.92$) parameters are provided for time- and temperature-resolved gasifier CFD-simulation.
(3) Chemical char characterization supports and underlines reactivity-modelling relationships and provide structure information on carbon actives sites. Char deactivation is induced by loss of functional groups (FT-IR), but more dominantly by graphitization and the growth of ordered crystalline structures (XRD, Raman spectroscopy,). With increasing annealing temperature, a steadily declining FWHM of the D_1 band (Raman spectroscopy) is be detected indicating a pronounced graphitization which lead to lowered char conversion rates. The loss and clustering of remaining catalytic mineral matter (EDX, EVT-ICP-OES) promotes char deactivation.

CRediT authorship contribution statement

Weiss Naim: Writing – original draft, Visualization, Validation, Software, Project administration, Methodology, Investigation, Formal analysis, Data curation, Conceptualization. **Philipp Treu:** Writing – original draft, Visualization, Validation, Methodology, Investigation, Formal analysis, Data curation. **Matthias Dohrn:** Writing – review & editing, Visualization, Validation, Software, Investigation, Formal analysis, Data curation. **Erisa Saraçi:** Writing – review & editing, Resources. **Jan-Dierk Grunwaldt:** Writing – review & editing, Supervision, Resources. **Sebastian Fendt:** Writing – review & editing, Supervision, Resources, Funding acquisition. **Hartmut Spliethoff:** Writing – review & editing, Supervision, Resources, Funding acquisition.

Declaration of competing interest

The authors declare that they have no known competing financial interests or personal relationships that could have appeared to influence the work reported in this paper.

Acknowledgements

This work is part of the project VERENA (03EE5044B), supported by the Federal Ministry of Economic Affairs and Climate Action (BWMK) and partners from industry (e.g. RWE, Air Liquide, Schmidt'sche Schack, Clariant). The financial support is gratefully acknowledged. The authors further thank Andrea Hartung, Anja Mair, Leon Kayser (fuel analysis), Lisa Göddert, Michael Knecht, Tobias Netter (pyrolysis and reactivity experiments), Hendrik Mörtenkötter, Caro Heilmeier (ETV-ICP-OES), Dr. Thomas Zevaco (FT-IR), Prof. Silke Behrens (XRD) for their support and great collaboration.

Appendix A. Supplementary data

Supplementary data to this article can be found online at https://doi.org/10.1016/j.fuel.2024.133848.

Data availability

Data will be made available on request.

References

[1] Hanel A, Dieterich V, Bastek S, Spliethoff H, Fendt S. Entrained flow gasification-based biomass-to-X processes: An energetic and technical evaluation. Energ Conver Manage 2022;274:116424. https://doi.org/10.1016/j.enconman.2022.116424.
[2] Jaeger M, Mayer M. The Noell Conversion Process – a gasification process for the pollutant-free disposal of sewage sludge and the recovery of energy and materials. Water Sci Technol 2000:37–44.
[3] Dahmen N, Abeln J, Eberhard M, Kolb T, Leibold H, Sauer J, et al. The bioliq process for producing synthetic transportation fuels. WIREs Energy Environ 2017; 6. https://doi.org/10.1002/wene.236.
[4] Dossow M, Dieterich V, Hanel A, Spliethoff H, Fendt S. Improving carbon efficiency for an advanced Biomass-to-Liquid process using hydrogen and oxygen from electrolysis. Renew Sustain Energy Rev 2021;152:111670. https://doi.org/10.1016/j.rser.2021.111670.
[5] Bridgwater AV. Review of fast pyrolysis of biomass and product upgrading. Biomass Bioenergy 2012;38:68–94. https://doi.org/10.1016/j.biombioe.2011.01.048.
[6] Walter KM, Serrer M-A, Kleist W, Grunwaldt J-D. Continuous production of higher alcohols from synthesis gas and ethanol using Cs-modified CuO/ZnO/Al2O3 catalysts. Appl Catal A 2019;585:117150. https://doi.org/10.1016/j.apcata.2019.117150.
[7] Artz J, Müller TE, Thenert K, Kleinekorte J, Meys R, Sternberg A, et al. Sustainable Conversion of Carbon Dioxide: An Integrated Review of Catalysis and Life Cycle Assessment. Chem Rev 2018;118:434–504. https://doi.org/10.1021/acs.chemrev.7b00435.
[8] Dieterich V, Buttler A, Hanel A, Spliethoff H, Fendt S. Power-to-liquid via synthesis of methanol, DME or Fischer–Tropsch-fuels: a review. Energy Environ Sci 2020;13: 3207–52. https://doi.org/10.1039/D0EE01187H.
[9] Widjaya ER, Chen G, Bowtell L, Hills C. Gasification of non-woody biomass: A literature review. Renew Sustain Energy Rev 2018;89:184–93. https://doi.org/10.1016/j.rser.2018.03.023.
[10] Mahinpey N, Gomez A. Review of gasification fundamentals and new findings: Reactors, feedstock, and kinetic studies. Chem Eng Sci 2016;148:14–31. https://doi.org/10.1016/j.ces.2016.03.037.
[11] Yu J, Lucas JA, Wall TF. Formation of the structure of chars during devolatilization of pulverized coal and its thermoproperties: A review. Prog Energy Combust Sci 2007;33:135–70. https://doi.org/10.1016/j.pecs.2006.07.003.
[12] Septien S, Valin S, Peyrot M, Dupont C, Salvador S. Characterization of char and soot from millimetric wood particles pyrolysis in a drop tube reactor between 800°C and 1400°C. Fuel 2014;121:216–24. https://doi.org/10.1016/j.fuel.2013.12.026.
[13] Trubetskaya A, Larsen FH, Shchukarev A, Ståhl K, Umeki K. Potassium and soot interaction in fast biomass pyrolysis at high temperatures. Fuel 2018;225:89–94. https://doi.org/10.1016/j.fuel.2018.03.140.
[14] Guizani C, Jeguirim M, Valin S, Limousy L, Salvador S. Biomass Chars: The Effects of Pyrolysis Conditions on Their Morphology. Structure, Chemical Properties and Reactivity, Energies 2017;10:796. https://doi.org/10.3390/en10060796.
[15] Trubetskaya A, Jensen PA, Jensen AD, Garcia Llamas AD, Umeki K, Gardini D, et al. Effects of several types of biomass fuels on the yield, nanostructure and reactivity of soot from fast pyrolysis at high temperatures. Applied Energy 171 2016:468–82. https://doi.org/10.1016/j.apenergy.2016.02.127.
[16] Cetin E, Moghtaderi B, Gupta R, Wall T. Influence of pyrolysis conditions on the structure and gasification reactivity of biomass chars. Fuel 2004;83:2139–50. https://doi.org/10.1016/j.fuel.2004.05.008.
[17] Tremel A, Spliethoff H. Gasification kinetics during entrained flow gasification – Part I. Devolatilisation and char deactivation, Fuel 2013;103:663–71. https://doi.org/10.1016/j.fuel.2012.09.014.
[18] Russell NV, Gibbins JR, Man CK, Williamson J. Coal Char Thermal Deactivation under Pulverized Fuel Combustion Conditions. Energy Fuels 2000;14:883–8. https://doi.org/10.1021/ef990241w.
[19] Shim H-S, Hurt RH. Thermal Annealing of Chars from Diverse Organic Precursors under Combustion-like Conditions. Energy Fuels 2000;14:340–8. https://doi.org/10.1021/ef9901286.
[20] Zolin A, Jensen A, Dam-Johansen K. Kinetic analysis of char thermal deactivation. Proc Combust Inst 2000:2181–8.
[21] Senneca O, Apicella B, Heuer S, Schiemann M, Scherer V, Stanzione F, et al. Effects of CO2 on submicronic carbon particulate (soot) formed during coal pyrolysis in a drop tube reactor. Combust Flame 2016;172:302–8. https://doi.org/10.1016/j.combustflame.2016.07.023.
[22] Di Blasi C. Combustion and gasification rates of lignocellulosic chars. Prog Energy Combust Sci 2009;35:121–40. https://doi.org/10.1016/j.pecs.2008.08.001.
[23] Roncancio R, Gore JP. CO2 char gasification: A systematic review from 2014 to 2020. Energy Convers Manage: X 2021;10:100060. https://doi.org/10.1016/j.ecmx.2020.100060.
[24] Vorobiev N, Geier M, Schiemann M, Scherer V. Experimentation for char combustion kinetics measurements: Bias from char preparation. Fuel Process Technol 2016;151:155–65. https://doi.org/10.1016/j.fuproc.2016.05.005.
[25] Russell NV, Gibbins JR, Williamson J. Structural ordering in high temperature coal chars and the effect on reactivity. Fuel 1999:803–7.

[26] Halama S, Spliethoff H. Numerical simulation of entrained flow gasification: Reaction kinetics and char structure evolution. Fuel Process Technol 2015;138: 314–24. https://doi.org/10.1016/j.fuproc.2015.05.012.

[27] Steibel M, Halama S, Geißler A, Spliethoff H. Gasification kinetics of a bituminous coal at elevated pressures: Entrained flow experiments and numerical simulations. Fuel 2017;196:210–6. https://doi.org/10.1016/j.fuel.2017.01.098.

[28] Asadullah M, Zhang S, Min Z, Yimsiri P, Li C-Z. Effects of biomass char structure on its gasification reactivity. Bioresour Technol 2010;101:7935–43. https://doi.org/10.1016/j.biortech.2010.05.048.

[29] Senneca O, Cortese L. Thermal annealing of coal at high temperature and high pressure. Effects on fragmentation and on rate of combustion, gasification and oxy-combustion, Fuel 2014;116:221–8. https://doi.org/10.1016/j.fuel.2013.07.065.

[30] Netter T, Fendt S, Spliethoff H. A collection of model parameters describing the gasification behavior of different fuels under entrained flow conditions. Fuel 2021; 296:120536. https://doi.org/10.1016/j.fuel.2021.120536.

[31] Senneca O, Apicella B, Russo C, Cerciello F, Salatino P, Heuer S, et al. Pyrolysis and Thermal Annealing of Coal and Biomass in CO 2 -Rich Atmospheres. Energy Fuels 2018;32:10701–8. https://doi.org/10.1021/acs.energyfuels.8b02417.

[32] Lu L, Kong C, Sahajwalla V, Harris DJ. Char structural ordering during pyrolysis and combustion and its influence on char reactivity. Fuel 2002:1215–25.

[33] Senneca O, Russo P, Salatino P, Masi S. The relevance of thermal annealing to the evolution of coal char gasification reactivity. Carbon 1997:141–51.

[34] Salatino P, Senneca O, Masi S. Assessment of Thermodeactivation during Gasification of a Bituminous Coal Char. Energy Fuels 1999;13:1154–9. https://doi.org/10.1021/ef9900334.

[35] Phounglamcheik A, Wang L, Romar H, Kienzl N, Broström M, Ramser K, et al. Effects of Pyrolysis Conditions and Feedstocks on the Properties and Gasification Reactivity of Charcoal from Woodchips. Energy Fuels 2020;34:8353–65. https://doi.org/10.1021/acs.energyfuels.0c00592.

[36] Peralta D, Paterson N, Dugwell D, Kandiyoti R. Pyrolysis and CO2 Gasification of Chinese Coals in a High-Pressure Wire-Mesh Reactor under Conditions Relevant to Entrained-Flow Gasification. Energy Fuels 2005;19:532–7. https://doi.org/10.1021/ef049762w.

[37] Schneider C, Walker S, Phounglamcheik A, Umeki K, Kolb T. Effect of calcium dispersion and graphitization during high-temperature pyrolysis of beech wood char on the gasification rate with CO2. Fuel 2021;283:118826. https://doi.org/10.1016/j.fuel.2020.118826.

[38] Holland T, Fletcher TH, Senneca O. Review of Carbonaceous Annealing Effects on O 2 and CO 2 Coal Reactivity. Energy Fuels 2019;33:10415–34. https://doi.org/10.1021/acs.energyfuels.9b02698.

[39] Cai H-Y, Güell AJ, Chatzakis IN, Lim J-Y, Dugwell DR, Kandiyoti R. Combustion reactivity and morphological change in coal chars: effect of pyrolysis temperature, heating rate and pressure. Fuel 1996:15–24.

[40] M. Dall'Ora, P.A. Jensen, A.D. Jensen. Suspension Combustion of Wood: Influence of Pyrolysis Conditions on Char Yield, Morphology, and Reactivity. Energy Fuels 2008;22:2955–62. https://doi.org/10.1021/ef800136b.

[41] Fermoso J, Stevanov C, B. MOGHTADERI, B. Arias, C. Pevida, M.G. Plaza, F. Rubiera, J.J. Pis, High-pressure gasification reactivity of biomass chars produced at different temperatures. J Anal Appl Pyrol 2009;85:287–93. https://doi.org/10.1016/j.jaap.2008.09.017.

[42] Netter T, Geißler A, Spliethoff H. Determination of the Intrinsic Gasification Kinetics of a Bituminous Coal Including Product Gas Inhibition and Char Deactivation Under Entrained Flow Conditions. J Energy Res Technol 2020;142: 070913. https://doi.org/10.1115/1.4046142.

[43] Yip K, Xu M, Li C-Z, Jiang SP, Wu H. Biochar as a Fuel: 3. Mechanistic Understanding on Biochar Thermal Annealing at Mild Temperatures and Its Effect on Biochar Reactivity, Energy Fuels 2011;25:406–14. https://doi.org/10.1021/ef101472f.

[44] Mahapatra N, Kurian V, Wang B, Martens F, gupta R. Pyrolysis of asphaltenes in an atmospheric entrained flow reactor: A study on char characterization. Fuel 152 2015:29–37. https://doi.org/10.1016/j.fuel.2015.02.086.

[45] Feng B, Jensen A, Bhatia SK, Dam-Johansen K. Activation Energy Distribution of Thermal Annealing of a Bituminous Coal. Energy Fuels 2003;17:399–404. https://doi.org/10.1021/ef020108v.

[46] Zhang J, Chen C, Zhou A, Z.u. Rahman, X. Wang, D. Stojiljković, N. Manić, M. Vujanović, H. Tan. Morphology of char particles from coal pyrolysis in a pressurized entrained flow reactor: Effects of pressure and atmosphere. Energy 238 2022:121846. https://doi.org/10.1016/j.energy.2021.121846.

[47] Wu H, Bryant G, Benfell K, Wall T. An Experimental Study on the Effect of System Pressure on Char Structure of an Australian Bituminous Coal. Energy Fuels 2000; 14:282–90. https://doi.org/10.1021/ef990066j.

[48] Cetin E, Moghtaderi B, Gupta R, Wall TF. Biomass gasification kinetics: Influences of pressure and char structure. Combust Sci Technol 2005;177:765–91. https://doi.org/10.1080/00102200590917266.

[49] Wall TF, Liu G, Wu H, Roberts DG, Benfell KE, Gupta S, et al. The effects of pressure on coal reactions during pulverised coal combustion and gasification. Progress in Energy and Combustion Science; 2002. p. 405–33.

[50] Yu J, Harris D, Lucas J, Roberts D, Wu H, Wall T. Effect of Pressure on Char Formation during Pyrolysis of Pulverized Coal. Energy Fuels 2004;18:1346–53. https://doi.org/10.1021/ef030019y.

[51] Benfell KE, Liu G-S, Roberts DG, Harris DJ, Lucas JA, Bailey JG, et al. Modelling char combustion: the influence of parent coal petrography and pyrolysis pressure on the structure and intrinsic reactivity of its char. Proc Combust Inst 2000: 2233–41.

[52] Kapteijn F, Porre H, Moulijn JA. CO2 gasification of activated carbon catalyzed by earth alkaline elements. AIChE J 1986:691-.

[53] Struis RPWJ, von Scala C, Stucki S, Prins R. Gasification reactivity of charcoal with CO2. Part II: Metal catalysis as a function of conversion. Chem Eng Sci 2002: 3593–602.

[54] Moulijn JA, Cerfontain MB, Kapteijn F. Mechanism of the potassium catalysed gasification of carbon in CO2. Fuel 1984:1043–7.

[55] Dupont C, Jacob S, Marrakchy KO, Hognon C, Grateau M, Labalette F, et al. Da Silva Perez, How inorganic elements of biomass influence char steam gasification kinetics. Energy 109 2016:430–5. https://doi.org/10.1016/j.energy.2016.04.094.

[56] Zhu H, Wang X, Wang F, Yu G. In Situ Study on K 2 CO 3 -Catalyzed CO 2 Gasification of Coal Char: Interactions and Char Structure Evolution. Energy Fuels 2018;32:1320–7. https://doi.org/10.1021/acs.energyfuels.7b03255.

[57] Pflieger C, Lotz K, Hilse N, Berger CM, Schiemann M, Debiagi P, et al. Catalytic influence of mineral compounds on the reactivity of cellulose-derived char in O2-, CO2-, and H2O-containing atmospheres. Fuel 2021;287:119584. https://doi.org/10.1016/j.fuel.2020.119584.

[58] Zolin A, Jensen A, Jensen PA, Frandsen F, Dam-Johansen K. The Influence of Inorganic Materials on the Thermal Deactivation of Fuel Chars. Energy Fuels 2001; 15:1110–22. https://doi.org/10.1021/ef000288d.

[59] Trubetskaya A, Jensen PA, Jensen AD, Steibel M, Spliethoff H, Glarborg P, et al. Comparison of high temperature chars of wheat straw and rice husk with respect to chemistry, morphology and reactivity. Biomass Bioenergy 2016;86:76–87. https://doi.org/10.1016/j.biombioe.2016.01.017.

[60] Schneider C, Rincón Prat S, Kolb T. Determination of active sites during gasification of biomass char with CO2 using temperature-programmed desorption. In: Part 1: Methodology & desorption spectra, Fuel 267; 2020. p. 116726. https://doi.org/10.1016/j.fuel.2019.116726.

[61] Newalkar G, Iisa K, D'Amico AD, Sievers C, Agrawal P. Effect of Temperature, Pressure, and Residence Time on Pyrolysis of Pine in an Entrained Flow Reactor. Energy Fuels 2014;28:5144–57. https://doi.org/10.1021/ef5009715.

[62] Xu K, Hu S, Su S, Xu C, Sun L, Shuai C, et al. Study on Char Surface Active Sites and Their Relationship to Gasification Reactivity. Energy Fuels 2013;27:118–25. https://doi.org/10.1021/ef301455x.

[63] Yu J, Guo Q, Ding L, Gong Y, Yu G. Study on the effect of inherent AAEM on char structure evolution during coal pyrolysis by in-situ Raman and TG. Fuel 2021;292: 120406. https://doi.org/10.1016/j.fuel.2021.120406.

[64] Liu Y, Paskevicius M, Sofianos MV, Parkinson G, Li C-Z. In situ SAXS studies of the pore development in biochar during gasification. Carbon 2021;172:454–62. https://doi.org/10.1016/j.carbon.2020.10.028.

[65] Feng B, Bhatia SK, Barry JC. Variation of the Crystalline Structure of Coal Char during Gasification. Energy Fuels 2003;17:744–54. https://doi.org/10.1021/ef0202541.

[66] Sadezky A, Muckenhuber H, Grothe H, Niessner R, Pöschl U. Raman microspectroscopy of soot and related carbonaceous materials: Spectral analysis and structural information. Carbon 2005;43:1731–42. https://doi.org/10.1016/j.carbon.2005.02.018.

[67] Shirsath AB, Mokashi M, Lott P, Müller H, Pashminehazar R, Sheppard T, et al. Soot Formation in Methane Pyrolysis Reactor: Modeling Soot Growth and Particle Characterization. J Phys Chem A 2023;127:2136–47. https://doi.org/10.1021/acs.jpca.2c06878.

[68] Liu G, Rezaei HR, Lucas JA, Harris DJ, Wall TF. Modelling of a pressurised entrained flow coal gasifier: the effect of reaction kinetics and char structure. Fuel 2000:1767–79.

[69] Senneca O, Ontyd C, Cerciello F, Schiemann M, Scherer V. Extension of the Thermal Annealing Concepts Developed for Coal Combustion to Conversion of Lignocellulosic Biomass. Energy Fuels 2020;34:3661–70. https://doi.org/10.1021/acs.energyfuels.9b03172.

[70] Zhang L, Huang J, Fang Y, Wang Y. Gasification Reactivity and Kinetics of Typical Chinese Anthracite Chars with Steam and CO 2. Energy Fuels 2006;20:1201–10. https://doi.org/10.1021/ef050343o.

[71] Mörtenkötter H, Grünwald D, Fendt S, Spliethoff H. Validation of Electrothermal Vaporization for the Analysis of Biomass Samples and Comparison with Other Methods of Analysis. Waste Biomass Valor 2023. https://doi.org/10.1007/s12649-023-02129-0.

[72] Senneca O, Salatino P. Loss of gasification reactivity toward O2 and CO2 upon heat treatment of carbons. Proc Combust Inst 2002:485–93.

[73] Sieradzka M, Mlonka-Mędrala A, Kalemba-Rec I, Reinmöller M, Küster F, Kalawa W, et al. Evaluation of Physical and Chemical Properties of Residue from Gasification of Biomass Wastes. Energies 2022;15:3539. https://doi.org/10.3390/en15103539.

[74] Droussi Z, D'orazio V, Provenzano MR, Hafidi M, Ouatmane A. Study of the biodegradation and transformation of olive-mill residues during composting using FTIR spectroscopy and differential scanning calorimetry. J Hazard Mater 2009; 164:1281–5. https://doi.org/10.1016/j.jhazmat.2008.09.081.

[75] Yang T, Meng J, Jeyakumar P, Cao T, Liu Z, He T, et al. Effect of pyrolysis temperature on the bioavailability of heavy metals in rice straw-derived biochar. Environ Sci Pollut Res Int 2021;28:2198–208. https://doi.org/10.1007/s11356-020-10193-5.

[76] Solomon PR, Carangelo RM. FTIR analaysis of coal. 1. Techniques and determination of hydroxyl concentrations. Fuel 1982:663–9.

[77] Reinmöller M, Schreiner M, Laabs M, Scharm C, Yao Z, Guhl S, et al. Formation and transformation of mineral phases in biomass ashes and evaluation of the feedstocks for application in high-temperature processes. Renew Energy 2023;210:627–39. https://doi.org/10.1016/j.renene.2023.04.072.

[78] Frigge L, Ströhle J, Epple B. Release of sulfur and chlorine gas species during coal combustion and pyrolysis in an entrained flow reactor. Fuel 2017;201:105–10. https://doi.org/10.1016/j.fuel.2016.11.037.

Glossary

Symbol: **Description & Unit**
d_i: inner diameter / mm
A_i: relative char reactivity of gasifying agent i / −
$dX\ dt^{-1}$: char conversion rate / g g^{-1} s^{-1}
E_A: activation energy kJ mol^{-1}
F_0: pre-exponential factor (deactivation model) s^{-1}
k_0: pre-exponential factor (Arrhenius equation) s^{-1}
L: length / mm
m: mass / g
r: reactivity / g g^{-1} s^{-1}
t: time / s
X: char conversion / −
Subscripts: **Description**
CO_2: carbon dioxide
deact: deactivated char
fresh: fresh char
K: potassium
KBr: potassium bromide
KCl: potassium chloride
O_2: oxygen
P: phosphor
Si: silica

Abbreviations: **Description**
AI: Alkali Index
ar: as-received
CFD: Computational fluid dynamics
daf: dry and ash free
DME: dimethyl ether
ETV-ICP-OES: Electro-thermal evaporation with inductively coupled plasma optical emission spectrometry
FT-IR: Fourier-Transform Infrared-Spectroscopy
FWHM: Full-width-half-maximum
HRTEM: High resolution transmission electron microscopy
LHV: Lower heating value
MtG: Methanol-to-gasoline
MtO: Methanol-to-olefins
NMR: Nuclear magnetic resonance spectroscopy
PiTER: High-pressure high-temperature entrained-flow reactor
SAF: Sustainable aviation fuels
SAXS: Small-angle X-ray scattering
SEM-EDX: Scanning electron microscope coupled to energy-dispersive X-ray spectroscopy
TEM: Transmission electron microscopy
TGA: Thermogravimetric analyzer
wf: water-free
XRD: X-ray diffraction
XRF: X-ray fluorescence spectroscopy